REPORT DOCUMENTATION PAGE

Form Approved OMB NO. 0704-0188

1. REPORT DATE (DD-MM-YYYY)	2. REPORT TYPE	3. DATES COVERED (From - To)
28-10-2018	Final Report	1-Sep-2011 - 31-May-2018

4. TITLE AND SUBTITLE
Final Report: PN Nanojunctions in Compound Semiconductors

5a. CONTRACT NUMBER
W911NF-11-1-0378

5b. GRANT NUMBER

5c. PROGRAM ELEMENT NUMBER
611102

6. AUTHORS

5d. PROJECT NUMBER

5e. TASK NUMBER

5f. WORK UNIT NUMBER

7. PERFORMING ORGANIZATION NAMES AND ADDRESSES

University of Rochester
ORPA
518 Hylan Building, RC Box 270140
Rochester, NY 14627 -0140

8. PERFORMING ORGANIZATION REPORT NUMBER

9. SPONSORING/MONITORING AGENCY NAME(S) AND ADDRESS (ES)

U.S. Army Research Office
P.O. Box 12211
Research Triangle Park, NC 27709-2211

10. SPONSOR/MONITOR'S ACRONYM(S)
ARO

11. SPONSOR/MONITOR'S REPORT NUMBER(S)
60124-EL.29

12. DISTRIBUTION AVAILIBILITY STATEMENT

Approved for public release; distribution is unlimited.

13. SUPPLEMENTARY NOTES

The views, opinions and/or findings contained in this report are those of the author(s) and should not contrued as an official Department of the Army position, policy or decision, unless so designated by other documentation.

14. ABSTRACT

15. SUBJECT TERMS

16. SECURITY CLASSIFICATION OF:			17. LIMITATION OF ABSTRACT	15. NUMBER OF PAGES	19a. NAME OF RESPONSIBLE PERSON
a. REPORT	b. ABSTRACT	c. THIS PAGE			Gary Wicks
UU	UU	UU	UU		19b. TELEPHONE NUMBER 585-275-4867

RPPR Final Report
as of 29-Oct-2018

Agency Code:

Proposal Number: 60124EL **Agreement Number: W911NF-11-1-0378**
INVESTIGATOR(S):

Name: Ph.D Gary Wicks Ph.D.
Email: wicks@optics.rochester.edu
Phone Number: 5852754867
Principal: Y

Organization: **University of Rochester**
Address: ORPA, Rochester, NY 146270140
Country: USA
DUNS Number: 041294109 EIN: 160743209
Report Date: 31-Aug-2018 Date Received: 28-Oct-2018
Final Report for Period Beginning 01-Sep-2011 and Ending 31-May-2018
Title: PN Nanojunctions in Compound Semiconductors
Begin Performance Period: 01-Sep-2011 **End Performance Period:** 31-May-2018
Report Term: 0-Other
Submitted By: Ph.D Gary Wicks Email: wicks@optics.rochester.edu
Phone: (585) 275-4867
Distribution Statement: 1-Approved for public release; distribution is unlimited.

STEM Degrees: 1 **STEM Participants:** 4

Major Goals: Major Goals of the Program

Overall Goal: Understanding and Suppression of Dark Current in MWIR Detectors
This was a fairly long program — after a few renewals, it last just short of 7 years (from Sept. 1, 2011 to May 31, 2018). The specific goals (individually discussed below) evolved over the duration of the program, but there was a constant central goal: understanding and suppression of dark current in mid-wave infrared (MWIR, 3-5 um) detectors.

Significance of the Problem of MWIR Detector Dark Current
Dark current and its noise-creating fluctuations are the major limitations of MWIR detector performance. MWIR detectors' dark current at room temperature is at least a million times greater, and often even quite a bit more than that, in comparison to SWIR (telecom) detectors. Thus dark current reduction is important aspect of MWIR detector research.

Approach
The problem of reducing dark currents is complicated by the fact that there are many different physical mechanisms that can produce dark current, and the dominant mechanism varies from detector to detector. Large device vs. small; MWIR vs. LWIR; superlattice vs. bulk material; room temperature vs. cooled. All these factors influence which dark current mechanism is the dominant one. A particular approach for reducing one type of dark current will usually be completely ineffective in reducing a different type of dark current. The is a need, addressed by this proposal, for comprehensive method to determine the dominant dark current mechanism and design devices to suppress it.

Step 1. Identify the Dark Current Mechanism
Our first step toward reducing dark current is identifying the physical mechanism that produces the dark current. At the beginning of this program, bulk dark current mechanisms in MWIR detectors were widely understood by the IR detector community, but surface current was poorly understood. A major goal of the present program was surface dark current: understanding its mechanisms and developing approaches to suppress it.

The process of identifying a particular dark current mechanism starts by imagining a qualitative description of the physical process, and then modeling the mechanism's dependence on experimental parameters that we have at our disposal, such as, applied voltage, temperature, defect concentration, and surface-to-volume ratio of the device. The final step is an examination of the dark current's dependence on the experimental parameters, and a

comparison with the model's predictions.

Step 2. Development of Device Architectures to Suppress the Dominant Dark Current Mechanism
Use of unipolar barrier heterostructures to suppress dark currents was first introduced by our lab in 2016 with the introduction of the nBn detector. This approach is still the best and most versatile, and is further applied in this program.
Initial Goal of the Program: Understanding and Controlling Surface Dark Current
The early efforts of the program concerned small devices. Since small devices have large surface to volume ratios, the small device task is essentially a surface current task. Later in the program, this investigation was generalized to include all III-V MWIR detectors, which are impaired by surface leakage currents.

The fundamental cause of surface leakage currents is that the materials' surface and bulk electrical characteristic are usually very different. Bulk characteristics of semiconductors are well understood. They are controlled by doping the material. But surface characteristics, and how to control them, were less understood at the beginning of the program. This is the main initial goal of the program

The importance of this initial effort on small devices is connected with several developments in IR detectors, for example:

- An ongoing trend in IR detector imaging arrays to move to smaller pixels
- Research in new detector materials and structures:

– quantum dots and quantum wires
– 2D semiconductors

It is the usual case that detectors are designed with the bulk characteristics in mind, surface characteristics are ignored, in part because (prior to this program) it wasn't known what the surface characteristics are or how to engineer them. In these cases, it is hit or miss as to whether the device will have surface leakage problems. At any rate, even if a large-sized version of the device works ok, if it is implemented in a small device, it is bound to be plagued by surface leakage.
Surface Electrical Characteristics of III-V Materials
The devices examined here are implemented in III-V semiconductor materials. Bulk electrical characteristics (conductivity type and magnitude) are engineering by doping with donors or acceptors. However, surface electrical characteristics are independent of doping, instead determined by surface fermi level pinning. The surface fermi level pinning location is a fundamental characteristic of each III-V material – some materials have the surface fermi level pinned in/near the conduction band and thus have n-type surfaces; some have the surface fermi level pinned near the valence band and have p-type surfaces.

Major initial goals of the program:
1. Develop and experimentally verify a method for predicting the individual surface electrical characteristics (surface fermi level pinning energy relative to the band edges) of the III-V materials and superlattices.
2. With this knowledge, develop device designs that engineer both bulk and surface characteristics for improved detector characteristics, for example, a detector design that blocks the flow of bulk and surface dark current.
Additional Goal: Detector Designs for Reduction of Bulk Dark Current
In the final few years of the program, through discussions with the program manager, William Clark, the program goals evolved to include dark current. The approach was similar to the initial approach to surface currents: first determine the physical mechanism of the dominant dark current, then develop device architectures to suppress it.

Defect-related Bulk Dark Currents
Bulk dark currents associated with defects are important for at least three reasons. First, despite the advanced technology of semiconductor crystal growth, no material is completely free of defects. Second, in space-based applications, detectors are exposed to radiation that creates defects, thereby degrading detector performance. Third, detector structures are increasingly being grown on large area, cheap substrates such as GaAs and Si. The detector epitaxial layers are mismatched to these substrates, and defects in the epitaxial layers result. These issues call for examining the mechanisms by which defects degrade detector performance, and designing detectors for optimized performance when elevated defects are present.

Reducing Dark Currents by Reducing Detector Volume
In the ideal scenario, a detector's dark current and performance is limited by diffusion current associated with Auger generation of minority carriers. To reach this goal, it is required to have a well-designed detector architecture and high quality materials. The goal is difficult, but some of today's detectors actually reach Auger-limited

performance. Once this goal is reached, further improvement in detector performance will require radical new concepts. One such concept involves reduction of the size of the detector, which reduces the dark current also. To be useful, the small detector must still be able to able most of the light.

An excellent approach is to insert a thin detector inside an optical cavity. Inside the optical cavity, light recirculates 100's of times, either by bouncing back and forth between two mirrors, or recirculating around a ring waveguide. The recirculating light passes through the detector 100's of times, enabling it to be 100's of times thinner, while absorbing most of the light. This reduction factor of the detector thickness will be the same factor by which the dark current is reduced.

Accomplishments: Accomplishment description uploaded as PDF document

Training Opportunities: Three PhD students participated in this research program, under the direct supervision of the PI. Two of the three students gave conference presentations.

Results Dissemination: Dissemination occurred via conference presentations and journal articles.

Honors and Awards: Nothing to Report

Protocol Activity Status:

Technology Transfer: A patent was filed and is pending. The patent title is "Low Dark Current Resonant Cavity Detector."

The patent has been licensed by Amethyst Research, Inc.

PARTICIPANTS:

Participant Type: PD/PI
Participant: Gary W Wicks
Person Months Worked: 12.00 **Funding Support:**
Project Contribution:
International Collaboration:
International Travel:
National Academy Member: N
Other Collaborators:

Participant Type: Graduate Student (research assistant)
Participant: Trevor O'Loughlin
Person Months Worked: 12.00 **Funding Support:**
Project Contribution:
International Collaboration:
International Travel:
National Academy Member: N
Other Collaborators:

Participant Type: Graduate Student (research assistant)
Participant: William Hughes
Person Months Worked: 12.00 **Funding Support:**
Project Contribution:
International Collaboration:
International Travel:
National Academy Member: N
Other Collaborators:

RPPR Final Report
as of 29-Oct-2018

Participant Type: Graduate Student (research assistant)
Participant: Xiaoyu Du
Person Months Worked: 6.00 **Funding Support:**
Project Contribution:
International Collaboration:
International Travel:
National Academy Member: N
Other Collaborators:

CONFERENCE PAPERS:

Publication Type: Conference Paper or Presentation **Publication Status:** 1-Published
Conference Name: SPIE Optical Engineering + Applications
Date Received: 25-Oct-2018 Conference Date: 28-Aug-2014 Date Published:
Conference Location: San Diego, California, United States
Paper Title: Effect of defects on III-V MWIR nBn detector performance
Authors: G. R. Savich, D. E. Sidor, X. Du, C. P. Morath, V. M. Cowan, and G. W. Wicks.
Acknowledged Federal Support: **Y**

Publication Type: Conference Paper or Presentation **Publication Status:** 1-Published
Conference Name: SPIE Defense + Security
Date Received: 30-Aug-2017 Conference Date: 06-May-2014 Date Published:
Conference Location: Baltimore, Maryland, USA
Paper Title: Defect-related dark currents in III-V MWIR nBn detectors
Authors: G. R. Savich, D. E. Sidor, X. Du, M. Jain, C. P. Morath, V. M. Cowan, J. K. Kim, J. F. Klem, D. Leonhard
Acknowledged Federal Support: **Y**

Publication Type: Conference Paper or Presentation **Publication Status:** 1-Published
Conference Name: SPIE Defense + Security
Date Received: 25-Oct-2018 Conference Date: 06-May-2014 Date Published:
Conference Location: Baltimore, Maryland, USA
Paper Title: Development of an ultrahigh-performance infrared detector platform for advanced spectroscopic sensing systems
Authors: Manish Jain, Gary Wicks, Andrew Marshall, Adam Craig, Terry Golding, Khalid Hossain, Ken McEwan, a
Acknowledged Federal Support: **Y**

Publication Type: Conference Paper or Presentation **Publication Status:** 1-Published
Conference Name: SPIE Defense + Security
Date Received: 30-Aug-2017 Conference Date: 31-Aug-2016 Date Published: 30-Sep-2016
Conference Location: Anaheim, California, United States
Paper Title: Effects of epitaxial structure and processing on electrical characteristics of InAs-based nBn infrared detectors
Authors: X. Du, G. R. Savich, B. T. Marozas, G. W. Wicks
Acknowledged Federal Support: **Y**

DISSERTATIONS:

RPPR Final Report
as of 29-Oct-2018

Publication Type: Thesis or Dissertation
Institution: University of Rochester
Date Received: 30-Aug-2017 Completion Date: 5/30/17 6:29PM
Title: Surface Conduction in III-V Semiconductor Infrared Detector Materials
Authors: Daniel Sidor
Acknowledged Federal Support: **N**

PATENTS:

Intellectual Property Type: Patent Date Received:
Patent Title: Low Dark Current, Resonant Cavity Enhanced Infrared Photodetectors
Patent Abstract: A resonant cavity-enhanced infrared photodetector has an absorber layer disposed between a fi
Patent Number: US2018/021910A1
Patent Country: USA
Application Date: 16-May-1916 Application Status: 2
Date Issued: 18-Jan-2018

Accomplishments

1. Surface Dark Current Studies

A. InAs

In order to learn about dark current mechanisms in InAs MWIR photodiodes, InAs pn junctions were grown by MBE and fabricated into test devices of a variety of mesa sizes from 25 µm to 500 µm. Electrical characteristics vs. temperature were measured. Bulk effects were identified by their scaling with the mesa area; surface effects scale with the mesa periphery. The InAs devices were found to exhibit bulk currents near room temperature, which transitions to surface currents at lower temperatures, as shown in figure 1.

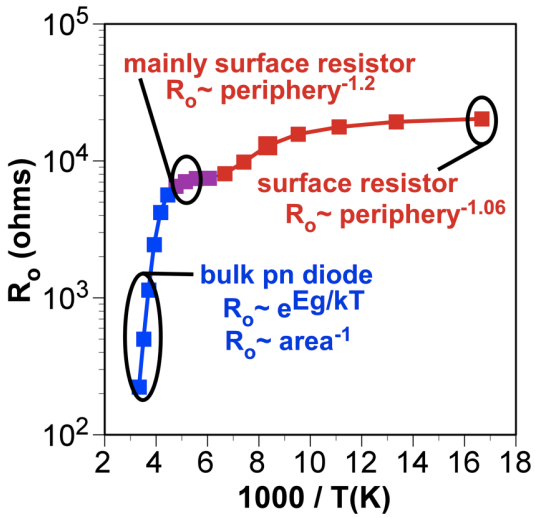

Figure 1. Zero-voltage resistance of a 200 micron mesa fabricated of an InAs pn epitaxial structure. The bulk region (blue) occurs at higher temperatures and is identified by the thermally activated dependence of the resistance on the bandgap and also the inverse dependence of the resistance on the mesa cross-sectional area. At lower temperatures, the resistance becomes surface dominated (red), identifiable by the temperature insensitivity and the inverse dependence on mesa periphery.

The temperature at which the dominant current mechanisms crosses over from bulk to surface is expected to be dependent on the size of the device mesa. This behavior was verified experimentally, as shown in figure 2.

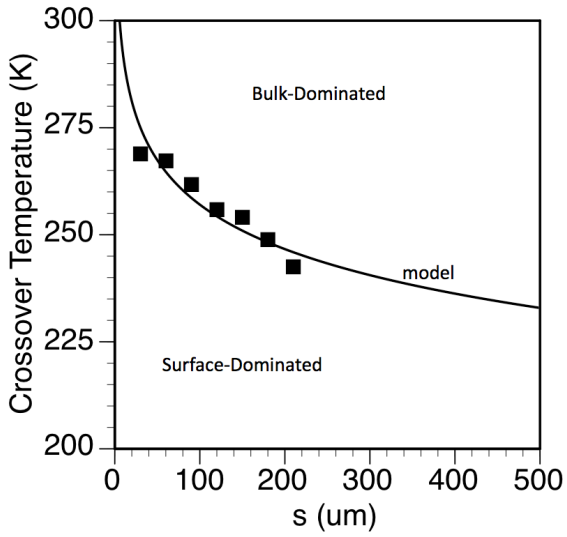

Figure 2. Bulk-surface crossover temperatures for the InAs pn mesas discussed in the text above. Surface-dominated behavior extends up to higher temperatures in smaller devices.

Figure 1 shows that bulk currents have a strong temperature dependence, dropping rapidly with cooling (resistance increasing with cooling), however surface currents are found to have a very weak temperature dependence. In common applications, the detector is cooled to reduce its dark current. Our findings indicate the optimum temperature of operation: the detector should be cooled to the point where the dark current transitions from bulk to surface current – further cooling beyond this point will yield little reduction in dark current. This optimum operating temperature will be dependent on the size of the detector, as indicated in figure 2.

There are two size regimes in common applications of InAs photodiodes. Single element detectors are typically made in sizes of 200-500 μm; individual pixels in imaging arrays are typically in the 20 μm range. Figure 2 shows that single element InAs photodiodes are optimally operated in the range of T~225-250K, whereas imaging areas of InAs photodiodes will not benefit much from cooling below T=275K. This represents a significant problem, as dark currents at T=275K are very large. The solution requires a reduction of surface currents.

B. InAs and GaSb

The previous work studying surface leakage in InAs was extended to another common III-V material employed in MWIR detectors, GaSb. Test pn junctions in both materials were grown by MBE and fabricated into mesa devices of a variety of sizes.

An Arrhenius plot of the zero bias conductance of both types of devices is shown in figure 3.

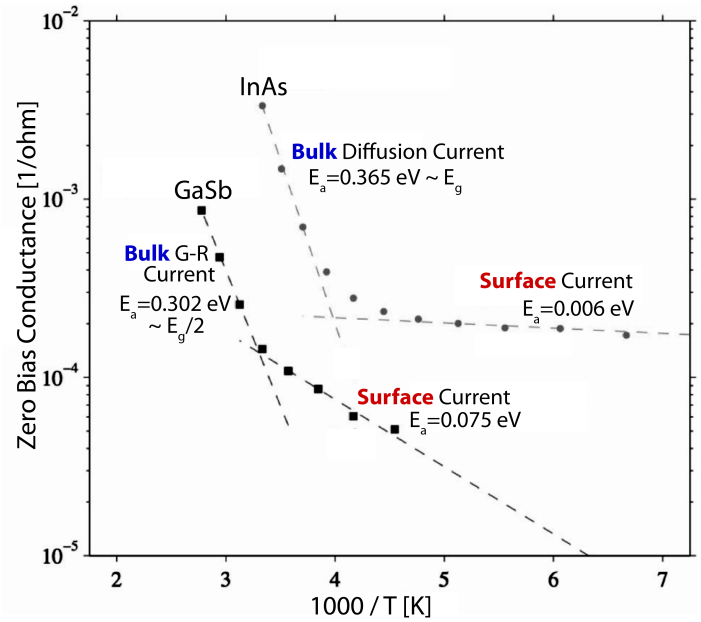

Figure 3. Arrhenius plot of InAs and GaSb pn junctions. At higher temperatures (near room temperature) the conduction mechanism is a bulk process: for InAs it is diffusion current as indicated by the full bandgap thermal activation energy; for GaSb it is generation-recombination current as indicated by the half-bandgap thermal activation energy. At lower temperatures, the conduction changes to a surface conduction, as indicated by the conductance scaling with the mesa periphery (figure 4). InAs's surface conduction is nearly independent of temperature whereas GaSb's surface conduction has a thermal activation energy of 0.075 eV.

To verify that the lower temperature currents are indeed surface currents, the dependence of the conductance on the size of the mesa was examined, as shown in figure 4.

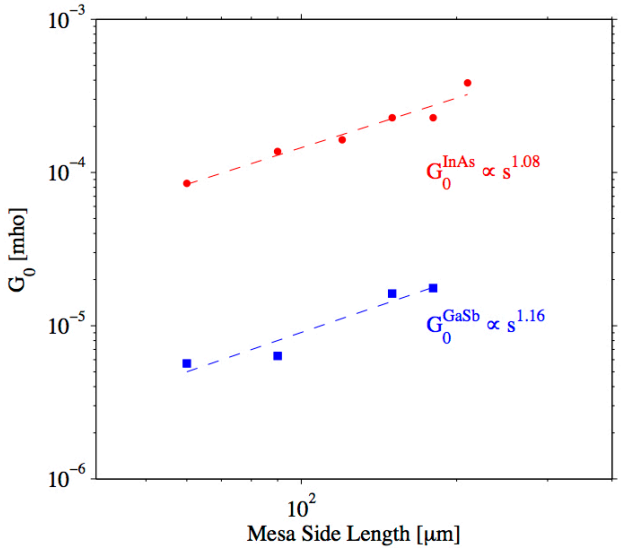

Figure 4. Size dependence T=200K zero bias differential conductance of InAs and GaSb pn test devices. Both conductances scale approximately with the length of the mesa, *i.e.,* scale with the periphery, indicating that the mechanism is a surface, rather than bulk, process.

As expected, these low temperature conductivities scale with the mesa side length, confirming that they are indeed surface leakage currents.

C. Generalized Description of Surface Electrical Characteristics of all III-V Materials and Superlattices

i. Binary Compounds

The understanding of surface dark currents starts with the realization that surface and bulk electrical characteristics are determined by completely different factors. Bulk electrical characteristics are determined by the doping – both the type (donor or acceptor) and the concentration. Modern semiconductor technology has well-developed control of doping, thus bulk electrical characteristics are able to be engineered very accurately. Surface characteristics of III-V materials, however, are *independent of doping*, instead being determined by *surface fermi level pinning.* Each particular III-V material has its surface fermi level pinned at an energy relative to its band edges that is a characteristic of the material. Surface electrical characteristics are not very engineerable – each particular material has its own surface characteristics.

Our above work on InAs and GaSb, as well as the work of others, indicates that the surface Fermi level of InAs is in the conduction band, producing a degenerate n-type surface, and the surface fermi level of GaSb is in the bandgap near the valence band, producing a non-degenerate p-type surface.

Surface fermi levels can be determined from the values of Schottky barrier heights, which are known for most of the III-V binary compounds. When showing the

location of the surface fermi levels of the III-V binaries on the same graph as the conduction and valence band edges, a remarkable picture emerges. *The surface fermi levels of the III-V binary compounds are all at approximately the same absolute energy,* as shown in figure 5.

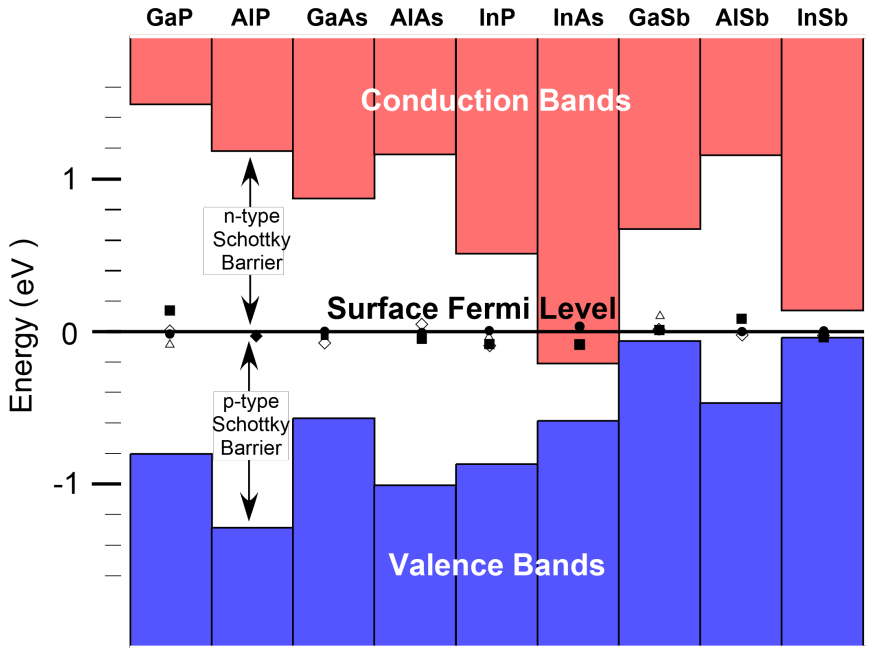

Figure 5. Surface fermi levels, as determined by measured values of Schottky barrier heights (data points shown on figure), and conduction and valence band energies of the III_V binary compounds. Band edges vary from one material to the next, but the surface fermi levels of all the materials are nearly at the same absolute energy.

The surface electrical characteristics are determined by the relationship between the surface fermi and the nearby band edge. If the surface fermi level is in or near the conduction band, the surface is n-type. If the surface fermi level is near the valence band, the surface is p-type. Since the surface fermi level is nearly constant, the surface electrical characteristics are mainly determined by the band edge energies: a material low energy conduction band (*e.g.*, InAs) will have an n-type surface and a material with a high energy valence band (*e.g.,* GaSb) will have a p-type surface. The larger bandgap materials (*e.g.,* GaAs) have neither a low conduction band or a high valence band, thus the surface fermi level is well within the bandgap producing a surface that is a depletion layer, *i.e.,* neither n-type or p-type.

The situation pictured in figure 5 creates five different types of surfaces, as shown in figure 6.

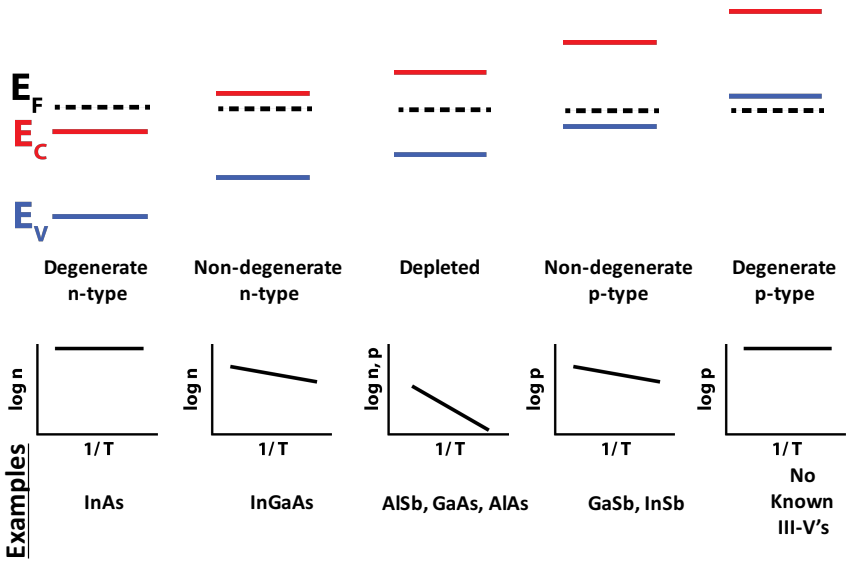

Figure 6. Five different types of surfaces, which depend on the energies of the band edges (which vary from one material to the next) relative to the fixed surface fermi level. Degenerate surfaces, such as that of InAs, will have electrical characteristics that are fairly independent of temperature. Non-degenerate surfaces will have electrical characteristics that have thermal activation energies that are equal to the energy difference between the surface fermi level and the nearby band edge.

The ideas displayed in figures 5 and 6 indicate that there is a close connection between the thermal activation energies of surface current, such as that shown in figures 1 and 3 above, and the energy of the band edge relative to the fixed surface fermi level. Because of its low (relative to the fixed surface fermi level) conduction band, InAs has a degenerate n-type surface with large, temperature-independent surface currents. The high valence band of GaSb produces a non-degenerate p-type surface with surface currents that have a thermal activiation energy equal to the energy separation of the surface fermi level and the valence band, about 0.075 eV. These descriptions are consistent with the measured characteristics of InAs and GaSb shown in figures 1-3 above.

The description of surface electrical characteristics described by figures 5 and 6 is consistent with electrical characteristics of surfaces of III-V binary compounds measured by us and many other groups. This picture's success for the binary compounds suggests that it could be more widely applied to ternary and quaternary compounds as well as superlattices.

ii. Ternary and Quaternary III-V Materials

The description of surface electrical characteristics described by figures 5 and 6 is consistent with electrical characteristics of surfaces of III-V binary compounds measured by us and many other groups. This picture's success for the binary compounds suggests that it could be more widely applied to III-V ternary and quaternary materials. The approach is similar to that used to describe the surface characteristics of the binary compounds: (1) assume that the surface fermi level is at

the same, constant absolute energy; (2) apply published data and/or models of others to determine the band edge energies; and (3) determine the relationship between the bands and the surface fermi level to determine the surface electrical characteristics. Figures 7 and 8 show this approach applied to two III-V alloys that are important MWIR and LWIR detector materials, InAsSb and GaInAsSb.

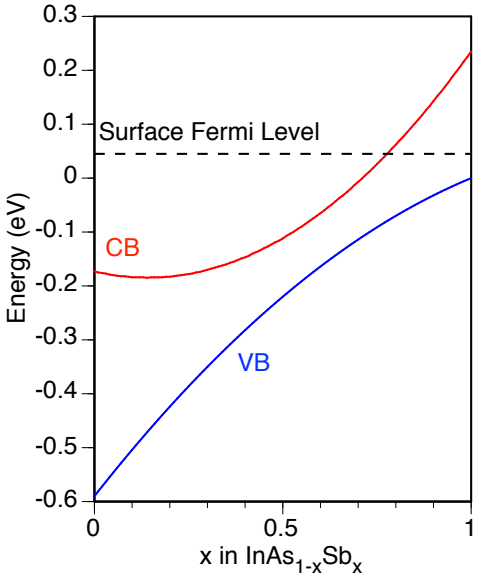

Figure 7. Band edges, calculated per Svennson, *et al*, relative to the expected constant surface Fermi level of InAsSb. The InAs endpoint has a degenerate n-type (surface Fermi level in conduction band) and the InSb endpoint has a non-degenerate p-type (surface Fermi level near valence band). Most of the composition range, $0 \le x \le 0.75$ has a degenerate n-type surface.

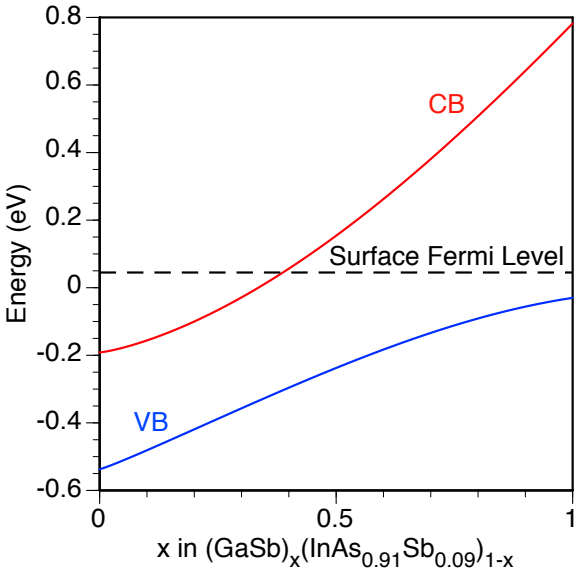

Figure 8. Band edges, calculated per Vergaftman, *et al*, relative to the expected constant surface Fermi level of GaInAsSb lattice-matched to GaSb substrates. The endpoints, $InAs_{0.91}Sb_{0.09}$ and GaSb, are seen to have surfaces that are degenerate n-type (surface Fermi level in conduction band) and non-degenerate p-type (surface Fermi level near valence band), respectively. The important e-SWIR compositions of x~0.7-0.8 are seen to have depleted surfaces (surface Fermi level near mid-gap).

The most important aspects of these findings are that InAs, InAsSb lattice-matched to GaSb, and LWIR InAsSb (mismatched to available substrates) all have degenerate n-type surfaces. InSb and GaSb have non-degenerate p-type surfaces.

iii. III-V Superlattices used for MWIR / LWIR detectors

In this section, we discuss the surface electrical characteristics of Ga containing superlattices (GaSb/InAs) and Ga-free superlattices (InAs/InAsSb).

Both materials of the Ga-free superlattice have degenerate n-type surfaces, as discussed above. Thus it seems reasonable to expect that the Ga-free superlattice will also have a degenerate n-type surface.

The Ga-containing superlattice is more complicated, however, in that one of its materials has an n-type surface and the other material has a p-type surface. How do we predict the result of combining these two dissimilar materials into a superlattice? The approach taken here is an extension of the above approach: (1) assume the same constant surface fermi level; (2) use results of others to specify the band energies; and (3) the surface electrical characteristics are determined from the relationship between the surface fermi level and the bands. The results for a Ga-containing superlattice and a Ga-free superlattice are shown in figure 9.

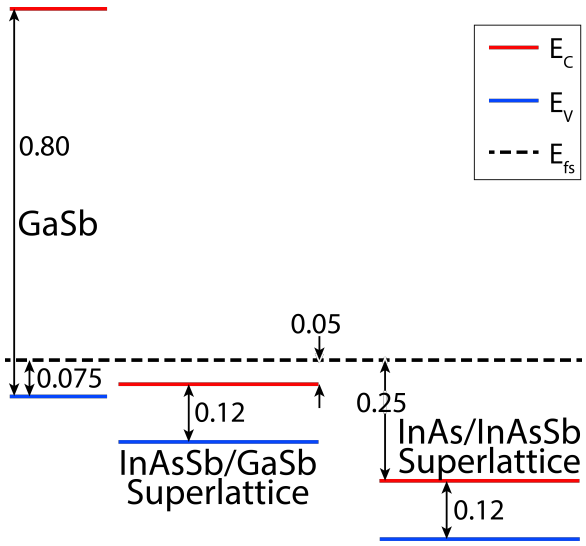

Figure 9. Band edges, E_C and E_V, and surface Fermi level, E_{fs} – all in units of eV. Shown are two representative superlattices that have 10 μm bandgap wavelengths at T=77K. Superlattice band edges relative to the GaSb E_V energy are calculated per Flatte, *et al*. The surface Fermi level, relative to the GaSb E_V energy, is known to be around 0.075 eV from figure 3. The surface Fermi level, relative to the band edges of the superlattices, is drawn under the assumption of an approximately constant surface Fermi level for the III-V materials and superlattices. The model predicts degenerate n-type surfaces for both superlattices.

Both examples of InAsSb/GaSb and InAs/InAsSb superlattices that were examined also have degenerate n-type surfaces, the former is barely degenerate and latter is strongly degenerate. It is expected that other InAsSb/GaSb superlattices with different layer thicknesses may not necessarily also have a degenerate surface, but it is likely that the surface will still be n-type. It is expected that all versions of InAs/InAsSb superlattices will have degenerate n-type surfaces (both of the constituent materials have degenerate n-type surfaces).

D. Detector Architectures and Surface Leakage

The nBn detector was originally demonstrated by our laboratory over a decade ago. These first nBn's spectacularly reduced surface currents to undetectable levels. The nBn name refers to the *bulk* doping of the layers, *i.e.,* the structure is two bulk n-type layers separated by a barrier. Those first nBn's were implemented in InAs-based materials and in $InAs_{0.91}Sb_{0.09}$-based materials. According to the above discussion, the surfaces of both InAs and $InAs_{0.91}Sb_{0.09}$-are n-type, *i.e.,* same conductivity type as

the bulk. Thus the bulk majority current and the surface current are both electron currents, and a single electron-blocking layer suppresses both.

The success of these initial nBn's in suppressing surface leakage suggested to some that all unipolar barrier architectures (of which the nBn is one) would automatically suppress surface leakage. This turned out to be false. Those working with superlattices for MWIR/LWIR detectors wanted to use p-type superlattices because of the superior transport characteristics of the minority carriers (electrons), hence they developed superlattice pBp detectors. Surprisingly and unfortunately, these detectors showed very large surface leakage. Initially this behavior was not understood, however we showed that it can be explained according to our above descriptions. The superlattices have n-type surfaces (figure 9), but the bulk layers in pBp's are doping p-type. The pBp device architecture employs a hole-blocking layer to block the bulk majority carriers. But this hole-blocking barrier will not block the electron currents flowing along the n-type surfaces, thus a large surface leakage current results.

The ability to predict the surface electrical characteristics of III-materials and superlattices, and its use in determining which types of unipolar barrier device architectures can suppress surface leakage current is a major success of this program.

2. Dark Currents Associated with Defects in pn-based Photodiodes and Unipolar Barrier Detectors

Infrared detectors with the nBn architecture or related unipolar barrier architectures perform differently in the presence of elevated defect concentrations when compared to conventional pn-junction based photodiodes. We show here the unipolar barrier photodetectors are significantly more defect resistant that pn photodiodes.

There are several cases where defect concentrations may become elevated in devices used for infrared detection. Detectors utilized for space-based applications or used in radiation-filled environments may initially exhibit low defect concentrations, but radiation in the detector environment can increase defect concentrations significantly. Alternatively, use of strained layer superlattice materials or materials lattice mismatched to the substrate can increase the density of defects over simpler lattice-matched epitaxial layers.

In this study, we controllably introduced defects into pn-based and unipolar barrier MWIR photodetectors via lattice mismatch or by proton irradiation. Figure 10 shows the effect of varying the defect concentration caused by lattice mismatch with the substrate by varying the thickness of the metamorphic buffer layer.

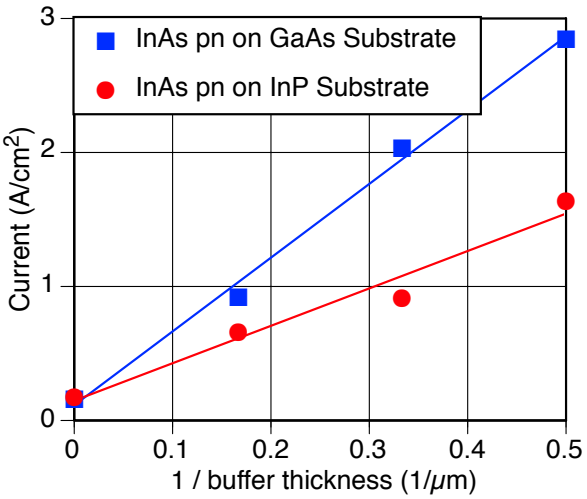

Figure 10. Current density vs. reciprocal buffer thickness for lattice mismatched InAs pn junction photodiodes on GaAs and InP substrates. A lattice-matched device is shown as a reciprocal buffer thickness of 0. Reciprocal buffer thickness is expected to be directly proportional to the density of defects that are associated with the lattice mismatch. Thus the horizontal axis is proportional to defect concentration. Dark current density is shown to be well fit by a direct proportionality to the defect density. The mismatch with GaAs is approximately twice the mismatch with InP, hence the lower dark currents on InP substrates.

The y-intercept point, indicated at zero reciprocal buffer thickness, or infinite buffer thickness, represent devices on lattice matched, InAs substrates. Since reciprocal buffer thickness is directly proportional to the defect density, fig. 10 shows that the dark current in mismatched pn photodiodes is directly proportional to the defect density, as expected by the Shockley-Read-Hall model. The lattice mismatch between InAs and GaAs is approximately twice that of the mismatch between InAs and InP, which causes elevated dark currents of the InAs photodiodes on GaAs substrates.

An Arrhenius plot of the dark current of the mismatched device on GaAs in figure 10 is compared with a lattice matched device in figure 11. The mismatch is seen to cause a 10x increase in dark current. The slopes of both plots are about the same, producing thermal activation energies equal to the bandgap, which is a defining characteristic of diffusion current.

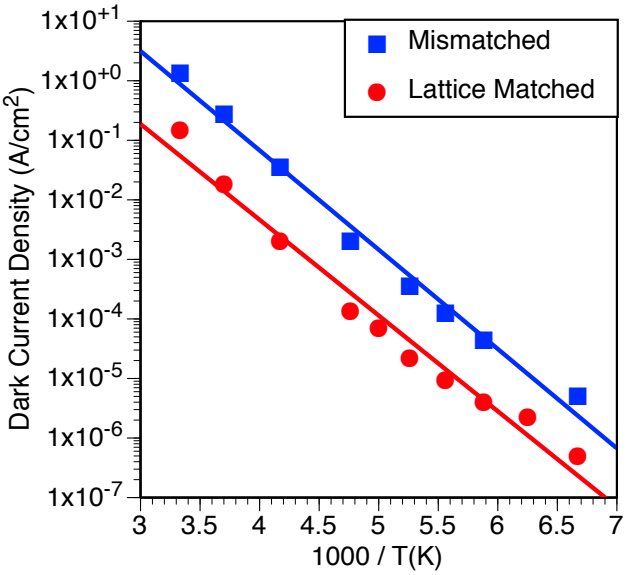

Figure 11. Arrhenius analysis for dark current density of both lattice matched and mismatched (on GaAs substrates) InAs nBn detectors. Both detectors exhibit diffusion limited performance, as indicated by the slope of the lines that indicated full bandgap thermal activation energies. Defects produced by the mismatch elevated the dark current by an order of magnitude.

The effects of defects in nBn detectors was compared with that of conventional pn-based detectors. Figure 12 shows an Arrhenius graph of dark currents of and InAs nBn and InAs pn, both grown mismatched on GaAs. At a typical operating temperature of these detectors around 200K, the nBn has a lower dark current by 10,000. The explanation is that the pn device device is dominated by defect-related g-r current, but the nBn device architecture avoids g-r current and remains diffusion limited.

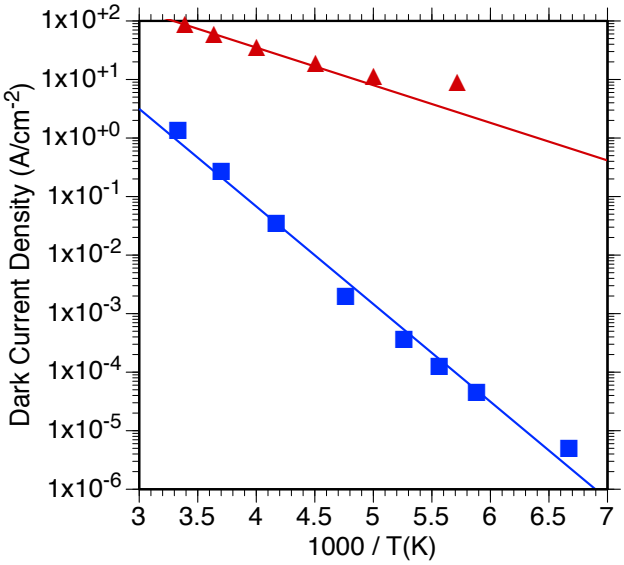

Figure 12. Arrhenius analysis for an InAs nBn detector (blue) and a conventional photodiode (red) grown on GaAs substrates. At a typical operating temperature of these detectors around 200K, the nBn has a lower dark current by 10,000.

In summary, in the presence of elevated defect concentrations, nBn detectors are dramatically more successful than pn-based detectors. Defects in nBn detectors create elevated dark currents but the devices remain diffusion-limited unlike conventional pn junction based photodiodes, which show significantly higher (several orders of magnitude) dark currents and g-r limited performance.

3. Suppressing Dark Currents Caused by Laterial Diffusion: the Inverted nBn Detector

Lateral diffusion of carriers increases dark current and degrades spatial resolution (modulation transfer function) of imaging arrays. We developed an inverted nBn structure to address these problems. Lateral diffusion in conventional nBn's can be eliminated by performing a deep etch (through the barrier layer and through the absorber layer), but this causes a new type of surface leakage current, trap-assisted tunneling along the barrier sidewall. We solved both problems of lateral diffusion and trap-assisted surface current by inverting the nBn structure, *i.e.* putting the barrier layer under the absorber. Now the absorber can be etched down to the barrier, eliminating the path of lateral diffusion, but the barrier layer is not etched, thus does not have an exposed sidewall, which eliminates trap-assisted tunneling surface currents. Figure 13 shows a comparison of a conventional shallow etched (etching the cap down to the barrier) nBn, a deep etched nBn, and an inverted nBn.

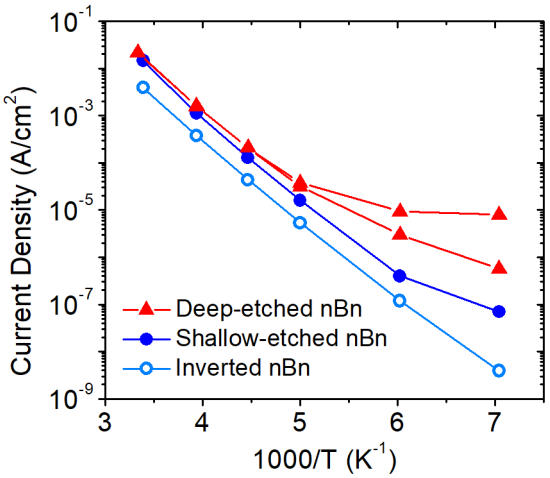

Figure 13. Arrhenius plot of current density at reverse bias of -0.4V for two deep-etched nBn devices, a shallow-etched nBn device and an inverted nBn device. All devices are of 180 μm × 180 μm. Deep-etched nBn devices show substantially higher dark current and lower thermal activation energy than the shallow-etched device at lower temperatures due to the surface TAT. Inverted nBn device is not subject to surface TAT and shows full-bandgap thermal activation energy at all temperatures.

Summary: the shallow etched nBn is subject to lateral diffusion; the deep etched nBn eliminated the pathway of lateral diffusion but exposes the barrier sidewall thereby creating trap assisted tunneling surface current; the inverted nBn solves both problems.

4. Ultra-High Performance Obtained MWIR / LWIR Detectors Using Intra-Cavity Designs

The usual mechanism that limits performance in MWIR and LWIR detectors is dark current. In this program, we have developed a new device architecture that produces substantial reductions in dark current. The concept is based on two facts:

1. In an optimized MWIR or LWIR detector, dark current is produced by thermal excitations across the semiconductors bandgap. The number of these thermal events scales with the volume of the active region of the detector. Thus, reducing the volume will reduce the dark current. However, if volume reduction results in less absorption of light (reduced quantum efficiency), the effort is counterproductive.
2. Detector volumes can be reduced without a loss of quantum efficiency by inserting the active region inside an optical cavity. Optical cavities can be created, in which light bounces back and forth 100's of times or more. Thus the active region of a detector placed inside the cavity will have 100's of chances to absorb light, thus it can be made 100's of times thinner. This reduction is thicker will produce a reduction in dark current.
3. Additional properties of these detectors in optical cavities: (1) the thinner detector will enable an increase in device speed due to reduction of carrier transit times; and (2) the optical cavity causes a narrow spectral response (as narrow as a few nm of wavelength) that is tunable, enabling spectroscopy to be performed by the detector.

We have designed two implementations of intracavity detectors.

A. Mirror-based Optical Cavity Detector.

The first method creates an optical cavity between two mirrors where incident light bounces back and forth many times. Inserted inside the optical cavity is a thin semiconductor absorbing layer, through which light passes many times, as shown in figure 14. The absorbing layer converts light into electrical output.

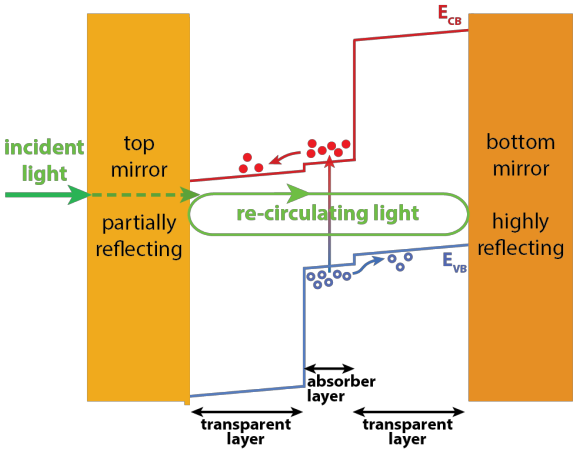

Figure 14. Schematic of a MWIR or LWIR Intra-Cavity Detector formed by two mirrors. Because of the light recirculation, the absorber layer can be very thin and still absorb most of the light. The thin absorber enables low dark current and high speed – both parameters are expected to be 100-1000× improvements over conventional IR detectors. An additional feature of the Resonant Cavity Detector is a narrow spectral bandwidth due to the interference of re-circulating light with itself – only a narrow range of wavelengths will interfere constructively.

B. Integrated Photonic Ring-Resonator Detector

The second method that we devised to create an intra-cavity detector uses integrated photonic ring-resonator structures. Such ring resonators are already commonplace in silicon-based photonic integrated circuits (although not yet with intra-cavity detectors).

The integrated photonic waveguides have a substantial amount of optical intensity just outside in the waveguide, in evanescent fields. The small volume detector will be placed at the waveguide surface, and the intensity in the evanescent fields will produce optical absorption in the detector, as shown in the figure 15.

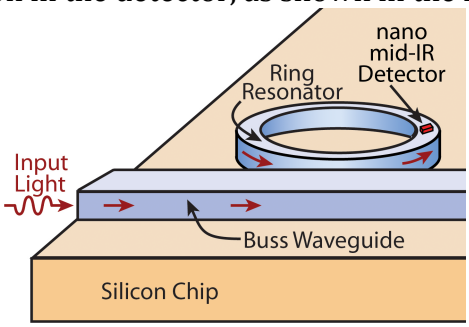

Figure 15. Schematic of a MWIR or LWIR Intra-Cavity Detector formed using an integrated photonic ring resonator. The small detector responds to the optical intensity in the evanescent fields at the edges of the integrated waveguide. The light recirculates hundreds of times around the ring resonator, provides many chances for the small detector to absorb light.

In both types of intracavity detectors, there can 100's of passes of the light through the small detector element. These multiple passes enable the use of absorber layers that are 100's of time thinner than in conventional detectors, while still absorbing

most of the light. The reduced detector thickness produces a similar reduction in dark current.

Dark Current
Dark current typically scales with the volume of the absorber layer, and thus is expected to be reduced by 100-1000× with respect to a conventional IR detector.

Speed
Minority carrier transit time across the absorber layer is the fundamental limitation of detector speed. The thinner absorber layer of the Resonant Cavity Detector is expected to increase speed by 100-1000×. (RC time constants need to be managed also, but they can engineered to allow multi-GHz performance).

Spectral Bandwidth
The recirculating light interferes with itself. Most wavelengths will not interfere constructively, thereby creating a spectrally narrow photoresponse. The spectral linewidth is determined by the number of re-circulations, which in turn is affected by the reflectivity of the mirrors. With high reflectivity mirrors (~99%), photoresponse as narrow $\Delta\lambda \sim$ a few nm is expected.

Background Current
The response of an IR detector to the ambient thermal background radiation can be a significant source of noise. The ambient background is spectrally broad, thus the spectrally broad response of a conventional IR detector can produce a sizable background current. The spectrally narrow response of the Resonant Cavity Detector will only respond to a thin slice of the background's spectrum, thereby reducing the background current. The reduction factor is roughly the ratio of the spectral widths of a conventional detector and a resonant cavity detector, which is on the order of 1000.

Initial Experimental Results
Figure 16 below shows the spectra of the wafer reflectivity and detector response of a mirror-based resonant cavity detector. The wafer reflectivity shows a large dip near the resonant wavelength of the optical cavity, and the detector response peaks

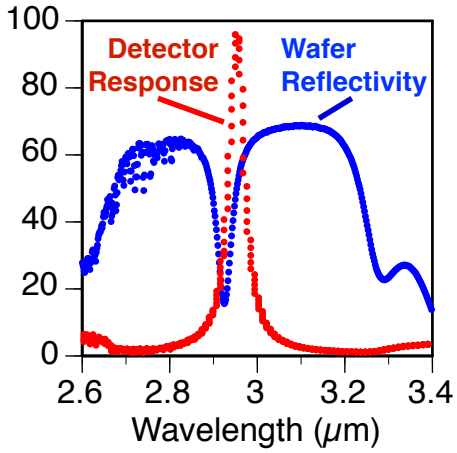

Figure 16. Initial experimental results of MWIR resonant cavity detector. The resonant wavelength of the cavity is seen as a large dip in the wafer reflectivity and a peak in the detector photo-response. The two spectral features are not exactly at the same wavelength because of wafer non-uniformity – the two measurements were made on different parts of the wafer.

at the cavity's resonant wavelength. The wafer was constructed of InAs-based materials grown by MBE.

We have demonstrated temperature tuning of a resonant cavity detector, shown in figure 17. Tunability over $\Delta\lambda \sim 50$ nm is measured.

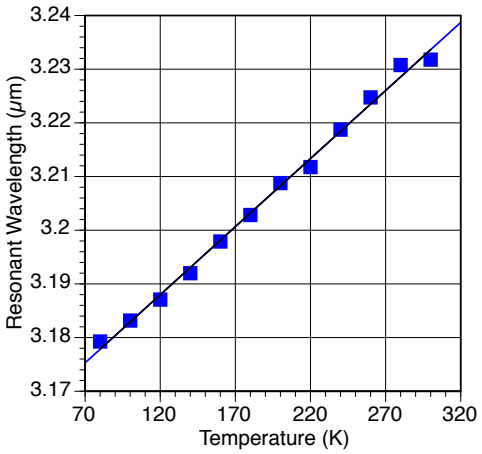

In summary, a new MWIR/LWIR detector concept is developed which will enable dramatic reductions in dark current and increases in device speed. The detector exhibits narrow spectral response (ideal for detecting laser sources and narrow absorption features of gases), which is tunable.